Cross-Domain Cascaded Deep Feature Translation

Oren Katzir
Tel-Aviv University

Dani Lischinski
Hebrew University of Jerusalem

Daniel Cohen-Or
Tel-Aviv University

Abstract

In recent years we have witnessed tremendous progress in unpaired image-to-image translation methods, propelled by the emergence of DNNs and adversarial training strategies. However, most existing methods focus on transfer of *style* and *appearance*, rather than on *shape* translation. The latter task is challenging, due to its intricate non-local nature, which calls for additional supervision. We mitigate this by descending the deep layers of a pre-trained network, where the deep features contain more semantics, and applying the translation from and between these deep features. Specifically, we leverage VGG, which is a classification network, pre-trained with large-scale semantic supervision. Our translation is performed in a cascaded, deep-to-shallow, fashion, along the deep feature hierarchy: we first translate between the deepest layers that encode the higher-level semantic content of the image, proceeding to translate the shallower layers, conditioned on the deeper ones. We show that our method is able to translate between different domains, which exhibit significantly different shapes. We evaluate our method both qualitatively and quantitatively and compare it to state-of-the-art image-to-image translation methods. Our code and trained models will be made available.

1 Introduction

In recent years, neural networks have significantly advanced generative image modeling. Following the emergence of Generative Adversarial Networks (GANs) [8], image-to-image translation methods have dramatically progressed, revolutionizing applications such as inpainting [37], super resolution [30], domain adaptation [10], and more. In particular, there have been intriguing advances in the setting of unpaired image-to-image translation through the use of cycle-consistency [35, 39] as well as other approaches [3, 13, 17, 22]. However, most existing methods acknowledge the difficulty in translating *shapes* from one domain to another, as this might entail highly non-trivial geometric deformations. Consider, for example, translating between elephants and giraffes, where we would expect the neck of an elephant to be extended, while the elephant's head should shrink. Furthermore, the challenge is compounded by the fact that, even within the same domain, images might exhibit extreme variations in object shape and pose, partial occlusions, and contain multiple instances of the object of interest. One might argue that this translation task is ill-posed to begin with, and at the very least, requires high-level semantics to be accounted for.

Nonetheless, several works do address shape deformation in the context of image-to-image translation by changing the architecture of the generative models [7] or requiring supervision in the form of segmentation [18, 25]. Recently, Wu at el. [31] propose to perform the translation by disentangling geometry and appearance, and assuming some intra-domain and inter-domain geometry consistency. All the above techniques, require the network to learn high-level semantics directly from the training data. However, this requires a large amount of training data, which might not be available for a specific unpaired translation task at hand.

In this paper, we address the problem of unpaired image-to-image translation between two different domains, where the objects of interest share some semantic similarity (e.g., four-legged mammals), whose shapes and appearances may, nevertheless, be drastically different. Our key idea is to

Figure 1: Given an image from domain A (zebras), we extract its deep features using a network pre-trained for classification, and translate them into deep features of domain B (giraffes). We use a cascade of deep-to-shallow adversarially trained translators, one for each deep feature layer.

accomplish the translation task by learning to translate between deep feature maps. Rather than learning to extract the relevant higher-level semantic information for the specific pair of domains at hand, we leverage deep features extracted by a network pre-trained for image classification, thereby benefiting from its large-scale fully supervised training.

Our work is motivated by the well-known observation that neurons in the deeper layers of pre-trained classification networks represent larger receptive fields in image space, and encode higher-level semantic content [38]. In other words, local activation patterns in the deeper layers may encode very different shapes in size and structure. Furthermore, Aberman et al. [1] showed that semantically similar regions from different domains, e.g. zebra and elephant, dog and cat, have similar activations. That is, the encoding of a cat's eye resembles that of a dog's eye more than that of its tail. From the point of view of the translation task, these properties are attractive, since they suggest that it might be possible to learn a *semantically consistent* translation between activation patterns produced by images from different domains, and that the resulting (reconstructed) image would be able to change drastically, hopefully bypassing the common difficulties in image-to-image translation methods.

More specifically, we learn to translate between several layers of deep feature maps, extracted from two domains by a pre-trained classification network, namely VGG-19 [26]. The translation is carried out one layer at a time in a deep-to-shallow (coarse-to-fine) *cascaded* manner. For each layer, we adversarially train a dedicated translator that acts in the features space of that layer. The deepest layer translator effectively learns to translate between semantically similar global structures, such as body shape or head position, as demonstrated by the middle pair of images in Figure 1. The translator of each shallower layer is conditioned on the translation result of the previous layer, and learns to add fine scale and appearance details, such as texture. At every layer, in order to visualize the generated deep features, we use a network pre-trained for inverting the deep features of VGG-19, following the method of Dosovitskiy and Brox [5]. The images shown in Figure 1 were generated in this manner.

We compare our method with several state-of-the-art image translation methods. To demonstrate the effectiveness of our approach, we present results for several challenging pairs of domains that exhibit drastically different shapes and appearances, but share some high-level semantics. Our translations are semantically consistent, typically preserving pose and number of instances of objects of interest, and reproducing their partial occlusion or cropping, as may be seen in Figure 5.

2   Related work

Zhu et al. [39] (simultaneously with [35] and [15]) has presented remarkable unpaired image-to-image translations, using a framework known as CycleGAN. The key idea is that the ill-posed conditional generative process can be regularized by a cycle-consistency constraint, which enforces the translation to perform bijective mapping. The cycle constraint has become a popular regularization technique for unpaired image-to-image translation. For example, the UNIT framework [21] assumes a shared latent space between the domains and enforces the cycle constraint in the shared latent space. Several works were developed to extend the one-to-one mapping to many-to-many mapping [22, 13, 17, 2]. These methods decompose the encoding space to shared latent space, representing the domain invariant content space, and domain specific style space. Therefore, many translations can be achieved from a single content code by changing the style code of the input image.

Many translation methods share the the inability to translate high-level semantics, including different shape geometry. This type of translation is usually necessary in the case of transfiguration, where one

aims to transform a specific type of objects without changing the background. Both [17] and [24] learn an attention map and apply translation only on the the foreground object. However, both methods only improve translations that do not deform shapes. Gokaslan et al. [7] succeed in preforming several shape-deforming translations by several modifications to the CycleGAN framework, including using dilated convolutions in the discriminator. However, they have not demonstrated strong shape deformations, such as zebras to elephants or giraffes, as we do in Section 4.

Liang et al. [18] and Mo et al. [25] assume some kind of segmentation is given, and used this segmentation to guide shape deformation translation. However, such segmentation is hard to achieve. In a recent work, Wu et al. [31] disentangle the input images to geometry and appearance spaces, relying on high intra-consistency, learning to translate each of the two domains separately.

Contrary to the above works, our work leverages a pre-trained network and the translation is applied directly on deep feature maps, thus being guided by high-level semantics. Several image-to-image methods, such as [34, 4, 14], also incorporate such pre-trained networks, though usually, only as perceptual loss, constraining the translated image to remain semantically close to the input image. Differently, Sungatullina et al. [27] incorporate pre-trained VGG features into the discriminator architecture, to assist in the discrimination phase. Wu et al. [32] use VGG-19 as a fixed encoder in the translation, where only the decoder is learned. Upchurch et al. [29] present the only method, to our knowledge, that actually translates deep features between two domains. However, the translation is not learned, but defined by simply interpolating between the deep features, which restricts the scope of method to highly aligned domains. For completeness, we also mention that Yin et al. [36] train an autoencoder to embed point clouds, and perform translation in the learned embedding. In contrast, we utilize semantics to preform the translation in the much more difficult scenario of images.

Our work shares some similarities with the early work of Huang et al. [12], which suggests using a generative adversarial model [8] in a coarse-to-fine manner with respect to a pre-trained encoder. The generation process begins from the deepest features and then recursively synthesizes shallower layers conditioned on the deeper layer, until generating the final image. This method was only applied on small encoders and low resolution images and was not explored for very deep and semantic encoding neural networks such as VGG-19 [26].

Deep image analogies [19] transfer visual attributes between semantically similar images, by feed-forwarding them through a pre-trained network. Their work does not train a generative model; nonetheless, they create new deep features by fusing content features from one image with style features of another. Similarly, Aberman et al. [1] synthesize hybrid images from two aligned images by selecting the dominant deep features response.

3 Method

Our general setting is similar to that of previous unpaired image-to-image translation methods. Given images from two domains, A and B, our goal is to learn to translate between them. However, unlike other image-to-image translation methods, we perform the translation on the deep features extracted by a pre-trained classification network, specifically VGG-19 [26].

The translation is carried out in a deep-to-shallow (coarse-to-fine) manner, using a cascade of pairs of translators, one pair per layer. The entire architecture used to train the translators is shown schematically in Figure 2, while Figure 3 illustrates the test-time translation (inference) process. Once the deepest feature map has been translated, we translate the next (shallower and less semantic feature map), conditioned on the translated deeper layer. In this manner, the translation of the shallower map preserves the general structure of the translated deeper one, but adds finer details, which are not encoded in the deeper feature maps. We repeat this procedure until the original image level is reached. Below we describe the training and the inference processes in more detail.

Pre-processing: We extract high-level semantic features from input images from both domains, A and B, by feed-forwarding the images through the pre-trained VGG-19 [26] network. Next, we sample five of the resulting deep feature maps, specifically `conv_i_1` ($i = 1, 2, 3, 4, 5$), where each map has progressively coarser spatial resolution, but a larger number channels. We denote the i-th sampled feature map for image $a \in A$ as a_i. Since propagation through the pre-trained VGG-19 network may yields features in any range, to ease the translation, we first normalize each channel, of every layer i, by calculating its mean and standard deviation across the domain and then we clamp
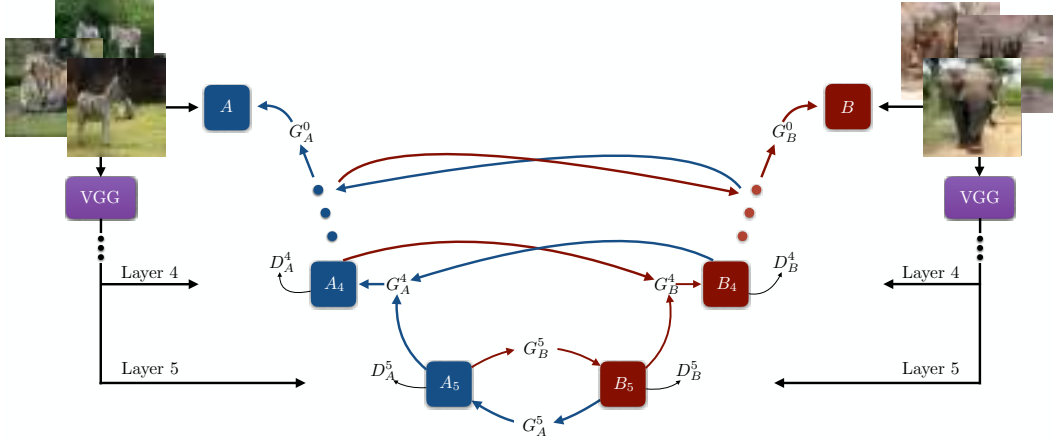
Figure 2: Translation architecture. We translate between domains A and B starting from the deepest feature maps A_5 and B_5, which encode the highest level semantic content of the images. Translation proceeds from deeper to shallower feature maps until reaching the image itself. The feature maps are extracted by feed forwarding every image through the pre-trained VGG-19 network and sampling five of its layers. Every layer's translation is learned individually, conditioned on the translation result of the next deeper layer (except the deepest layer, whose translation is unconditional).
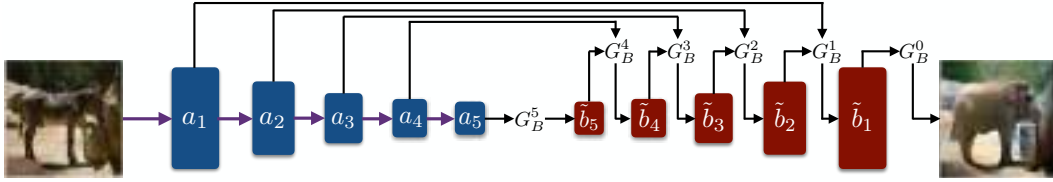

Figure 3: Translation of the top left image at test time. The input image is fed forward through VGG-19 layers, as indicated by the right purple arrows. Then, starting from the deepest layer a_5 we translate each layer. The final result is obtained from the shallowest layer using feature inversion.

the normalized feature values to the range of $[-1, 1]$. While the clamping is an irreversible operation, we did not observe any adverse effect on the results. We use A_i (B_i) to denote set of all normalized deep feature maps of level i, extracted from images in domain A (B).

Inference: We perform the translation in a coarse-to-fine fashion. Thus, the translator from domain A to B, actually consists of a sequence of translators $\{G_B^5, G_B^4, \ldots, G_B^1\}$, where each translator is responsible for translating the i-th feature map layer a_i, from A_i to B_i conditioned on the previously translated deeper layer $\tilde{b}_{i+1}$ (except for the deepest layer translator G_B^5, which is unconditioned). Finally, G_B^0 uses feature inversion to convert $\tilde{b}_1$ to obtain the translated image. The translators G_A^i from domain B_i to A_i are defined symmetrically. The entire inference pipeline is shown in Figure 3.

Feature inversion: In all the results we show, e.g., Figure 1, we visualize the output of the various translators by pre-training a deep feature inversion network (per domain), for each layer $i = 1, \ldots, 5$, following Dosovitskiy and Brox [5]. The network aims to reconstruct the original image given the feature map of a specific layer, regularized by adversarial loss so that the reconstructed image would lie in the manifold of natural images. For more details we refer the reader to [5]. The specific settings used in our implementation are elaborated in the supplementary materials.

Deepest layer translation: We begin by translating the deepest feature maps, encoding the highest-level semantic features, i.e., A_5 and B_5, hence, our problem is reduced to translating high-dimensional tensors. Our solution builds upon the commonly used CycleGAN framework [39]. Specifically, we use the three losses proposed in [39]. First, in order to generate deep features in the appropriate domain, we utilize an adversarial domain loss $\mathcal{L}_{adv}$. We simultaneously train two translators G_A^5, G_B^5 which try to fool domain-specific discriminators, D_A^5, D_B^5 (for domains A_5, B_5, respectively). However,

4

differently from [39] and other image translation methods [13, 25], we have found LSGAN [23] not to be well-suited for our task, leading to mode collapse or convergence failures. Instead, we found WGAN-GP [9] more effective, thus, the adversarial loss for translation from X to Y is defined as

$$\mathcal{L}_{adv}\left(G_Y, D_Y, X, Y\right) = \mathop{\mathbb{E}}_{x \sim \mathbb{P}_X}\left[D_Y\left(G_Y\left(x\right)\right)\right] - \mathop{\mathbb{E}}_{y \sim \mathbb{P}_Y}\left[D_Y\left(y\right)\right] + \lambda_{gp}\mathop{\mathbb{E}}_{\hat{y} \sim \mathbb{P}_{\hat{Y}}}\left[\left(\|\nabla D_Y\left(\hat{y}\right)\| - 1\right)^2\right], \quad (1)$$

where $G_Y : X \to Y$ is the translator, D_Y is the target domain discriminator, $\lambda_{gp} = 10$ in all our experiments, and $\mathbb{P}_{\hat{Y}}$ is defined by uniformly sampling along straight lines between $\tilde{y} \sim G\left(\mathbb{P}_X\right)$ and $y \sim \mathbb{P}_Y$. For more details we refer the reader to [9].

Second, for regularizing the translation to one-to-one mapping, we add the cycle constraint,

$$\mathcal{L}_{cyc}(G_X, G_Y, X, Y) = \mathop{\mathbb{E}}_{x \sim \mathbb{P}_X}\|G_X\left(G_Y\left(x\right)\right) - x\| + \mathop{\mathbb{E}}_{y \sim \mathbb{P}_Y}\|G_Y\left(G_X\left(y\right)\right) - x\|, \quad (2)$$

where $\|\cdot\|$ stands for the L_1 norm.

Finally, we also use the identity loss, which guides the networks to preserve common high level features,

$$\mathcal{L}_{idty}(G_X, G_Y, X, Y) = \mathop{\mathbb{E}}_{x \sim \mathbb{P}_X}\|G_X\left(x\right) - x\| + \mathop{\mathbb{E}}_{y \sim \mathbb{P}_Y}\|G_Y\left(y\right) - y\|. \quad (3)$$

The entire loss combines these components as follows

$$\begin{aligned}\mathcal{L}^5 =&\mathcal{L}_{adv}\left(G_B^5, D_B^5, A_5, B_5\right) + \mathcal{L}_{adv}\left(G_A^5, D_A^5, B_5, A_5\right) \\ &+ \lambda_{cyc}\mathcal{L}_{cyc}(G_A^5, G_B^5, A_5, B_5) + \lambda_{idty}\mathcal{L}_{idty}(G_A^5, G_B^5, A_5, B_5),\end{aligned} \quad (4)$$

where λ_{cyc} and λ_{idty} were set to 100 in all our experiments.

Coarse to fine conditional translation: Consider two successive layers, $a_i \in A_i$ and $a_{i+1} \in A_{i+1}$, where the latter has already been translated, yielding $\tilde{b}_{i+1}$ as the translation outcome (see Figure 3). We next perform the translation of the layer a_i to yield $\tilde{b}_i$, using the translator G_B^i, conditioned on $\tilde{b}^{i+1}$. Note that G_B^i is effectively a function of all the previously translated layers.

The architecture of G_B^i is schematically shown in Figure 4. Since shallower layers encode less of the semantic content of the image, it is more difficult to learn how they should be deformed, and thus they are used to transfer "style", while the "content" comes from the already translated deeper layer. Inspired by Huang et al. [13], we add an adaptive instance normalization (AdaIN) [11] component, whose parameters are learned from the current layer. Thus, several layers of G_B^i are normalized according to the AdaIN component. G_A^i, which is designed symmetrically, is learned simultaneously with G_B^i, as shown in Fig.4(a).

The loss for training these shallower translators is roughly the same as that used for training the deepest translation: it consists of adversarial domain loss, cycle constraint loss, and identity loss. While we formalize the adversarial loss unconditionally, similarly to (1), the cyclic loss is now conditioned: $\left\|G_A^i\left(G_B^i\left(a_i, \tilde{b}_{i+1}\right), a_{i+1}\right) - a_i\right\| + \left\|G_B^i\left(G_A^i\left(b_i, \tilde{a}_{i+1}\right), b_{i+1}\right) - b_i\right\|$, and the same is true for the identity loss $\left\|G_A^i\left(a_i, a_{i+1}\right) - a_i\right\| + \left\|G_B^i\left(b_i, b_{i+1}\right) - b_i\right\|$.

We train the pairs of translators one layer at a time, starting from G_A^5 and G_B^5. More details regarding the implementation and the training of the translators are included in the supplementary material.

4   Experiments

We evaluate our methods on several publicly available datasets: (1) Cat $\leftrightarrow$ dog faces [17], which contains 871 cats images and 1364 dogs images and does not require high shape deformation; (2) Kaggle Cat $\leftrightarrow$ dog [6] dataset with over $12,500$ images in each domain (the images may contain part of the object or several instances); (3) Challenging MSCOCO dataset [20], specifically, zebra $\leftrightarrow$ elephant and zebra $\leftrightarrow$ giraffe (the number of images is each category is reported in [20]). We note that no previous method has used MSCOCO, without supervision in the form of segmentation.

Our deepest translators, i.e., G_A^5, G_B^5, consist of encoder-decoder structure with several strided convolutional layers followed by symmetric transpose convolutional layers. We use group normalization [33] and ReLU activation function (except the last layer, which is `tanh`). The conditional
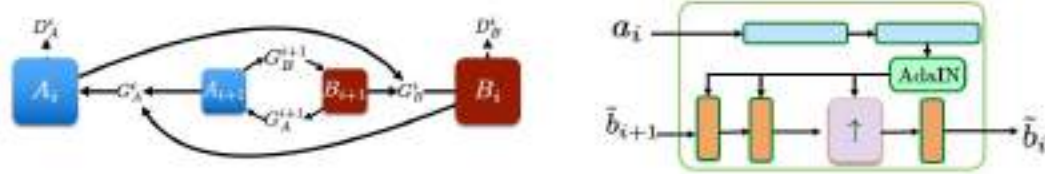
Figure 4: Translation of layer i is conditioned on the previously translated layer $i + 1$. The two translators G_A^i and G_B^i are trained simultaneously (see left figure), where $i + 1, \ldots, 5$ translators are fixed. On the right we show the schematic architecture of G_B^i which has two inputs: $a_i \in A_i$ and $\tilde{b}_{i+1}$. a_i is fed-forward through several layers to yield AdaIN parameters which control the generation of $\tilde{b}_i$. Since $\tilde{b}_i$ has twice the spatial size of $\tilde{b}_{i+1}$, we add an upsampling layer marked by $\uparrow$.

Figure 5: Examples of challenging translation results, featuring significant shape deformations.

generators, consist of learned AdaIN layer, achieved by several strided convolutional layers followed by fully connected layers. The content generator has also several convolutional layers and one single transpose convolutional layer which doubles the spatial resolution (Figure 4(right)). In practice we only train G^5, G^4, G^3, and apply feature inversion directly on the output of the latter, with negligible degradation. For the exact layer's specifics we refer the reader to our supplementary file and to our (soon to be published) code. We run each layer for 400 epochs with fixed learning rate of 0.0001 and Adam optimizer [16]. On a single RTX 2080 reaching the final image takes around 2.5 days, including the final inversion network training.

Several translation examples are presented in Figure 5. Our translation is able to achieve high shape deformation. Note that our translations are semantically consistent, in the sense that they preserve the pose of the object of interest, as well the the number of instances. Furthermore, partial occlusions of such objects, or their cropping by the image boundaries are correctly reproduced. See for example, the translations of the pairs of animals in columns 5–6. More results are provided in the supplementary material.

Figure 6: Translation of the 5th (deepest) layer with different loss combinations. Using all three components yields the best result.

Figure 7: Translation of different VGG layers, separately. Low level semantics translation fails to deform the geometry of the object.

Figure 8: Comparison to other image-to-image translation methods. The unpaired translations, from left to right, are zebra ↔ giraffe, elephant ↔ zebra and dog ↔ cat, where every translation has four examples, two in each direction. While previous translation methods struggle to deform the geometry of the source images, our method is able to preform drastic geometric deformation, while preserving the poses of the subjects and the overall composition of the image.

4.1 Ablation study

We analyze two main elements of our method. First, we validate the use of CycleGAN loss components. As shown in Figure 6, we translate the 5th (deepest) layer with and without cycle, identity and adversarial losses. The best approach is achieved by using all of the losses, which balance each other.

In addition, in Figure 7 we compare translation of different VGG-19 layers. Evidently, shallower layers introduce spatial constraints, thus, limiting the translation in the sense of shape's changes. The shallowest layer can hardly change the shape of the input image, which may explain the failure of end-to-end image translation methods. Additional results are presented in the supplementary file.

4.2 Comparison to other methods

We compare our result with leading image translation methods, i.e. CycleGAN [39], MUNIT [13], and DRIT [17].

Quantitative comparison: In order to perform a quantitative comparison, we use the common FID score, which measures the distance between features of pre-trained inception network [28]. The results of the comparison are reported in Table 1. Our method achieved the best FID score on five out of the six cross-domain translations for which this score was measured.

Qualitative comparison: In Figure 8 we show several challenging translation examples. While end-to-end methods struggle to preform translations with such drastic shape deformation, our method is able to do so, without additional supervision thanks to its use of the pre-trained VGG-19 network.

The success of our method can also be explained and visualized by examining the translated deep features. Since in all our experiments the image size was set to 224×224, we are able to feed forward

→/←	Cycle GAN	MUNIT	DRIT	Ours
Cat ↔ Dog	125.75/94.27	159.57/108.51	153.94/139.17	**67.58/46.02**
Zebra ↔ Giraffe	**55.65**/58.93	238.06/60.78	59.75/54.06	67.41/**39.38**
Zebra ↔ Elephant	86.55/68.44	109.56/80.1	78.01/56.39	**68.45/47.86**

Table 1: FID score comparison. We compare our FID scores against three approaches on three datasets, measured for both translation directions per dataset. The two directions appear side-by-side, →/←, at each cell.
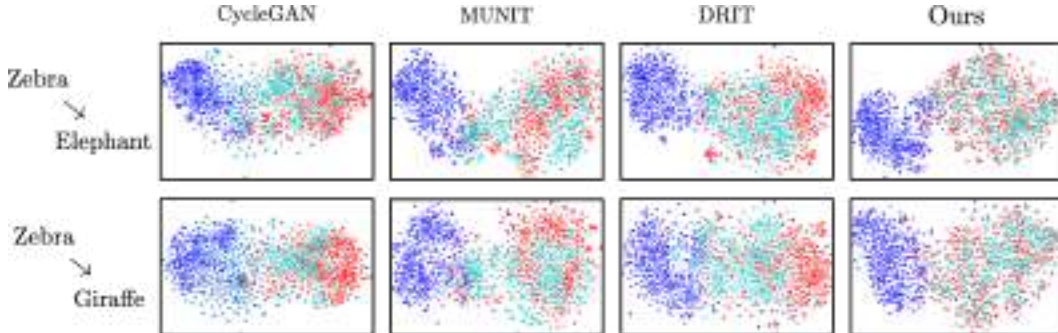

Figure 9: Comparison of the deepest latent spaces (5th layer), projected using t-SNE. The latent space of the source domain is in blue, and the target domain is in red. The translation results are plotted in cyan. The distribution of the translation results is most similar to that of the target domain when using our method.

all the images through the entire VGG network, including its final fully-connected layers. For every image, original and translated, we extract the last fully-connected layer (before the classification layer), which is a vector of size 4096. We project this vector to 2D, using t-SNE, as shown in Figure 9. The original feature vectors of the source and target domains are plotted in blue and red, respectively. The feature vectors of the translated results are plotted in cyan. It may be seen that the distribution of the translated vectors are closest to the original ones when using our method.

Limitations: Our method achieves translations with significant shape deformation in many previously unattainable scenarios, yet, a few limitations remain. First, the background of the object is not preserved, as the background is encoded in the deep features along with the semantic parts. Also, in some cases the translated deep features may be missing small instances or parts of the object. This may be attributed to the fact that VGG-19 is generally not invertible and was trained to classify finite set of classes. In addition, since we translate deep features, small errors in the deep translation may be amplified to large errors in the image, while for image-to-image translation method that operate on the image directly, small translation errors would typically be more local.

5 Conclusions

Translating between image domains that differ not only changes in appearance, but also exhibit significant geometric deformations, is a highly challenging task. We have presented a novel image-to-image translation scheme that operates directly on pre-trained deep features, where local activation patterns provide a rich semantic encoding of large image regions. Thus, translating between such patterns is capable of generating significant, yet semantically consistent, shape deformations. In a sense, this solution may be thought of as transfer learning, since we make use of features that were trained for a classification task for an unpaired translation task. In the future, we would like to continue exploring the applications of powerful pre-trained deep features for other challenging tasks, possibly in different domains, such as videos, sketches or 3D shapes.

References

[1] Kfir Aberman, Jing Liao, Mingyi Shi, Dani Lischinski, Baoquan Chen, and Daniel Cohen-Or. Neural best-buddies: Sparse cross-domain correspondence. *ACM Transactions on Graphics (TOG)*, 37(4):69, 2018.

[2] Amjad Almahairi, Sai Rajeswar, Alessandro Sordoni, Philip Bachman, and Aaron Courville. Augmented CycleGAN: Learning many-to-many mappings from unpaired data. *arXiv preprint arXiv:1802.10151*, 2018.

[3] Sagie Benaim and Lior Wolf. One-sided unsupervised domain mapping. In *Advances in neural information processing systems*, pages 752–762, 2017.

[4] Xing Di, Vishwanath A Sindagi, and Vishal M Patel. GP-GAN: Gender preserving GAN for synthesizing faces from landmarks. In *2018 24th International Conference on Pattern Recognition (ICPR)*, pages 1079–1084. IEEE, 2018.

[5] Alexey Dosovitskiy and Thomas Brox. Generating images with perceptual similarity metrics based on deep networks. In *Advances in neural information processing systems*, pages 658–666, 2016.

[6] Jeremy Elson, John JD Douceur, Jon Howell, and Jared Saul. Asirra: a CAPTCHA that exploits interest-aligned manual image categorization. In *ACM Conference on Computer and Communications Security*, 2007.

[7] Aaron Gokaslan, Vivek Ramanujan, Daniel Ritchie, Kwang In Kim, and James Tompkin. Improving shape deformation in unsupervised image-to-image translation. In *Proceedings of the European Conference on Computer Vision (ECCV)*, pages 649–665, 2018.

[8] Ian Goodfellow, Jean Pouget-Abadie, Mehdi Mirza, Bing Xu, David Warde-Farley, Sherjil Ozair, Aaron Courville, and Yoshua Bengio. Generative adversarial nets. In *Advances in neural information processing systems*, pages 2672–2680, 2014.

[9] Ishaan Gulrajani, Faruk Ahmed, Martin Arjovsky, Vincent Dumoulin, and Aaron C Courville. Improved training of Wasserstein GANs. In *Advances in Neural Information Processing Systems*, pages 5767–5777, 2017.

[10] Judy Hoffman, Eric Tzeng, Taesung Park, Jun-Yan Zhu, Phillip Isola, Kate Saenko, Alexei A Efros, and Trevor Darrell. Cycada: Cycle-consistent adversarial domain adaptation. *arXiv preprint arXiv:1711.03213*, 2017.

[11] Xun Huang and Serge Belongie. Arbitrary style transfer in real-time with adaptive instance normalization. In *Proceedings of the IEEE International Conference on Computer Vision*, pages 1501–1510, 2017.

[12] Xun Huang, Yixuan Li, Omid Poursaeed, John Hopcroft, and Serge Belongie. Stacked generative adversarial networks. In *Proceedings of the IEEE Conference on Computer Vision and Pattern Recognition*, pages 5077–5086, 2017.

[13] Xun Huang, Ming-Yu Liu, Serge Belongie, and Jan Kautz. Multimodal unsupervised image-to-image translation. In *Proceedings of the European Conference on Computer Vision (ECCV)*, pages 172–189, 2018.

[14] Andrey Ignatov, Nikolay Kobyshev, Radu Timofte, Kenneth Vanhoey, and Luc Van Gool. Wespe: weakly supervised photo enhancer for digital cameras. In *Proceedings of the IEEE Conference on Computer Vision and Pattern Recognition Workshops*, pages 691–700, 2018.

[15] Taeksoo Kim, Moonsu Cha, Hyunsoo Kim, Jung Kwon Lee, and Jiwon Kim. Learning to discover cross-domain relations with generative adversarial networks. In *Proceedings of the 34th International Conference on Machine Learning-Volume 70*, pages 1857–1865. JMLR. org, 2017.

[16] Diederik P. Kingma and Jimmy Ba. Adam: A method for stochastic optimization. *CoRR*, abs/1412.6980, 2014.

[17] Hsin-Ying Lee, Hung-Yu Tseng, Jia-Bin Huang, Maneesh Singh, and Ming-Hsuan Yang. Diverse image-to-image translation via disentangled representations. In *Proceedings of the European Conference on Computer Vision (ECCV)*, pages 35–51, 2018.

[18] Xiaodan Liang, Hao Zhang, Liang Lin, and Eric Xing. Generative semantic manipulation with mask-contrasting gan. In *Proceedings of the European Conference on Computer Vision (ECCV)*, pages 558–573, 2018.

[19] Jing Liao, Yuan Yao, Lu Yuan, Gang Hua, and Sing Bing Kang. Visual attribute transfer through deep image analogy. *arXiv preprint arXiv:1705.01088*, 2017.

[20] Tsung-Yi Lin, Michael Maire, Serge Belongie, James Hays, Pietro Perona, Deva Ramanan, Piotr Dollár, and C Lawrence Zitnick. Microsoft COCO: Common objects in context. In *European conference on computer vision*, pages 740–755. Springer, 2014.

[21] Ming-Yu Liu, Thomas Breuel, and Jan Kautz. Unsupervised image-to-image translation networks. In *Advances in Neural Information Processing Systems*, pages 700–708, 2017.

[22] Liqian Ma, Xu Jia, Stamatios Georgoulis, Tinne Tuytelaars, and Luc Van Gool. Exemplar guided unsupervised image-to-image translation. *arXiv preprint arXiv:1805.11145*, 2018.

[23] Xudong Mao, Qing Li, Haoran Xie, Raymond YK Lau, Zhen Wang, and Stephen Paul Smolley. Least squares generative adversarial networks. In *Proceedings of the IEEE International Conference on Computer*

Vision, pages 2794–2802, 2017.

[24] Youssef Alami Mejjati, Christian Richardt, James Tompkin, Darren Cosker, and Kwang In Kim. Unsupervised attention-guided image-to-image translation. In *Advances in Neural Information Processing Systems*, pages 3693–3703, 2018.

[25] Sangwoo Mo, Minsu Cho, and Jinwoo Shin. Instagan: Instance-aware image-to-image translation. *arXiv preprint arXiv:1812.10889*, 2018.

[26] Karen Simonyan and Andrew Zisserman. Very deep convolutional networks for large-scale image recognition. *arXiv preprint arXiv:1409.1556*, 2014.

[27] Diana Sungatullina, Egor Zakharov, Dmitry Ulyanov, and Victor Lempitsky. Image manipulation with perceptual discriminators. In *Proceedings of the European Conference on Computer Vision (ECCV)*, pages 579–595, 2018.

[28] Christian Szegedy, Wei Liu, Yangqing Jia, Pierre Sermanet, Scott Reed, Dragomir Anguelov, Dumitru Erhan, Vincent Vanhoucke, and Andrew Rabinovich. Going deeper with convolutions. In *Proceedings of the IEEE conference on computer vision and pattern recognition*, pages 1–9, 2015.

[29] Paul Upchurch, Jacob Gardner, Geoff Pleiss, Robert Pless, Noah Snavely, Kavita Bala, and Kilian Weinberger. Deep feature interpolation for image content changes. In *Proceedings of the IEEE conference on computer vision and pattern recognition*, pages 7064–7073, 2017.

[30] Xintao Wang, Ke Yu, Shixiang Wu, Jinjin Gu, Yihao Liu, Chao Dong, Yu Qiao, and Chen Change Loy. Esrgan: Enhanced super-resolution generative adversarial networks. In *Proceedings of the European Conference on Computer Vision (ECCV)*, pages 0–0, 2018.

[31] Wayne Wu, Kaidi Cao, Cheng Li, Chen Qian, and Chen Change Loy. TransGaGa: Geometry-aware unsupervised image-to-image translation. *arXiv preprint arXiv:1904.09571*, 2019.

[32] Xuehui Wu, Jie Shao, Lianli Gao, and Heng Tao Shen. Unpaired image-to-image translation from shared deep space. In *2018 25th IEEE International Conference on Image Processing (ICIP)*, pages 2127–2131. IEEE, 2018.

[33] Yuxin Wu and Kaiming He. Group normalization. In *Proceedings of the European Conference on Computer Vision (ECCV)*, pages 3–19, 2018.

[34] Jingjing Xu, Xu Sun, Qi Zeng, Xuancheng Ren, Xiaodong Zhang, Houfeng Wang, and Wenjie Li. Unpaired sentiment-to-sentiment translation: A cycled reinforcement learning approach. *arXiv preprint arXiv:1805.05181*, 2018.

[35] Zili Yi, Hao Zhang, Ping Tan, and Minglun Gong. Dualgan: Unsupervised dual learning for image-to-image translation. In *Proc. IEEE ICCV*, pages 2849–2857, 2017.

[36] Kangxue Yin, Zhiqin Chen, Hui Huang, Daniel Cohen-Or, and Hao Zhang. Logan: Unpaired shape transform in latent overcomplete space. *arXiv preprint arXiv:1903.10170*, 2019.

[37] Jiahui Yu, Zhe Lin, Jimei Yang, Xiaohui Shen, Xin Lu, and Thomas S Huang. Free-form image inpainting with gated convolution. *arXiv preprint arXiv:1806.03589*, 2018.

[38] Matthew D Zeiler and Rob Fergus. Visualizing and understanding convolutional networks. In *European conference on computer vision*, pages 818–833. Springer, 2014.

[39] Jun-Yan Zhu, Taesung Park, Phillip Isola, and Alexei A Efros. Unpaired image-to-image translation using cycle-consistent adversarial networks. In *Proc. IEEE ICCV*, pages 2223–2232, 2017.

6 Supplementary Material

6.1 Training details

6.1.1 Hyper parameters

In all our experiments, unless stated otherwise, we use Adam optimizer [16] with $\beta_1 = 0.5, \beta_2 = 0.999$. The learning rate was set to 0.0001 and the batch size to 10. During training, random crop and image mirroring is applied. Our training methodology follows WGAN-GP [9], thus for one generator update we update the discriminator four times.

6.1.2 Network architecture

Feature Inversion   Our implementation is similar to Dosovitskiy and Brox [5]. We train an individual feature inversion network for VGG layer, where each layer has different channels (512, 512, 256, 128, 64). All layers utilize Leaky ReLU nonlinearity (0.2) and employ no normalization. The last layer utilizes Tanh. All inversion networks, first apply three non-strided convolutional layers, with N input number of channels, equal to the number of channels each deep layer has. Next, several transpose convolutional layers are applied, each doubles the resolution of the image and decreases the channel resolution (by factor of 2) until the image resolution 224 is achieved (thus, different amount of ConvTranspose layers per layer). The final layer is a non-strided convolutional layer followed by Tanh layer. Together they project the features back to the original image dimensions and range (number of output channels is 3). For the discriminator we have used Patch GAN discriminator, with four strided convolutional layers, each utilizes batch normalization (except the first one) and Leaky ReLU. For the adversarial metric, only here, we have used LS-GAN. Here we also set the batch size to 25.

Deepest layer translation   The input to the deepest translation network is `conv_5_1`, thus, the input size is $14 \times 14 \times 512$ (recall the input image size is 224×224). The identity and cycle losses are multiplied by $\lambda_{idty} = \lambda_{cyc} = 100$. The architecture is reported in Table.S1. The networks is relatively small and achieve good results in a few hours on a single GPU (RTX2080). We use the WGAN-GP optimization method, updating the generator once for every four discriminator updates.

Name	Input ch.	Output ch.	Kernel sz.	Stride	GN
conv	512	512	3	1	no
conv	512	256	3	2	yes
relu	-	-	-	-	-
conv	256	512	3	2	yes
relu	-	-	-	-	-
convT	512	256	3	2	yes
relu	-	-	-	-	-
convT	256	256	3	2	yes
relu	-	-	-	-	-
conv	256	512	3	1	yes
relu	-	-	-	-	-
conv	512	512	3	1	no
tanh	-	-	-	-	-

Table S1: Deepest layer translation architecture.

Coarse to fine conditional translation   The coarse-to-fine generator, for generating level i, has two inputs: the current source VGG level and the previous translated VGG features $(i + 1)$. An AdaIN component, acts on on the current deep features and normalizes several layers in the translator itself. We report the AdaIN component structure for generating layer four in Table.S2. The architecture can be extended easily to other layers. The core components of the translator, which takes as input the previous translated layer, are reported in Table.S3.

Name	Input ch.	Output ch.	Kernel sz.	Stride	GN
conv	512	512	3	2	no
lrelu	-	-	-	-	-
conv	512	512	3	2	no
lrelu	-	-	-	-	-
conv	512	512	3	2	no
lrelu	-	-	-	-	-
linear	$4 \times 4 \times 512$	1000	-	-	no
lrelu	-	-	-	-	
linear	1000	x	-	-	no

Table S2: AdaIN component for the second deepest layer. The output x is equal to the number of parameters the AdaIN normalizes. AdaIN for different VGG layer's translation are defined similarly, where we simply add more conv layer for each shallower VGG layer.

Name	Input ch.	Output ch.	Kernel sz.	Stride	AdaIN
conv	x	x	3	1	yes
lrelu	-	-	-	-	-
conv	x	x	3	1	yes
lrelu	-	-	-	-	-
convT	x	$x/2$	4	2	yes
lrelu	-	-	-	-	-
conv	$x/2$	$x/2$	3	1	no
tanh	-	-	-	-	-

Table S3: Coarse to fine translator. The input number of channels, x, varies according to the current VGG layer.

6.2 More comparison results

In this section we show more results, not presented in the paper, for zebra↔giraffe, zebra↔elephant and cat↔dog translations.

Original	Cycle GAN	MUNIT	DRIT	Ours

Figure S1: Qualitative comparisons. MSCOCO zebra to giraffe.

Original	Cycle GAN	MUNIT	DRIT	Ours

Figure S2: Qualitative comparisons. MSCOCO zebra to giraffe.

Original   Cycle GAN   MUNIT   DRIT   Ours
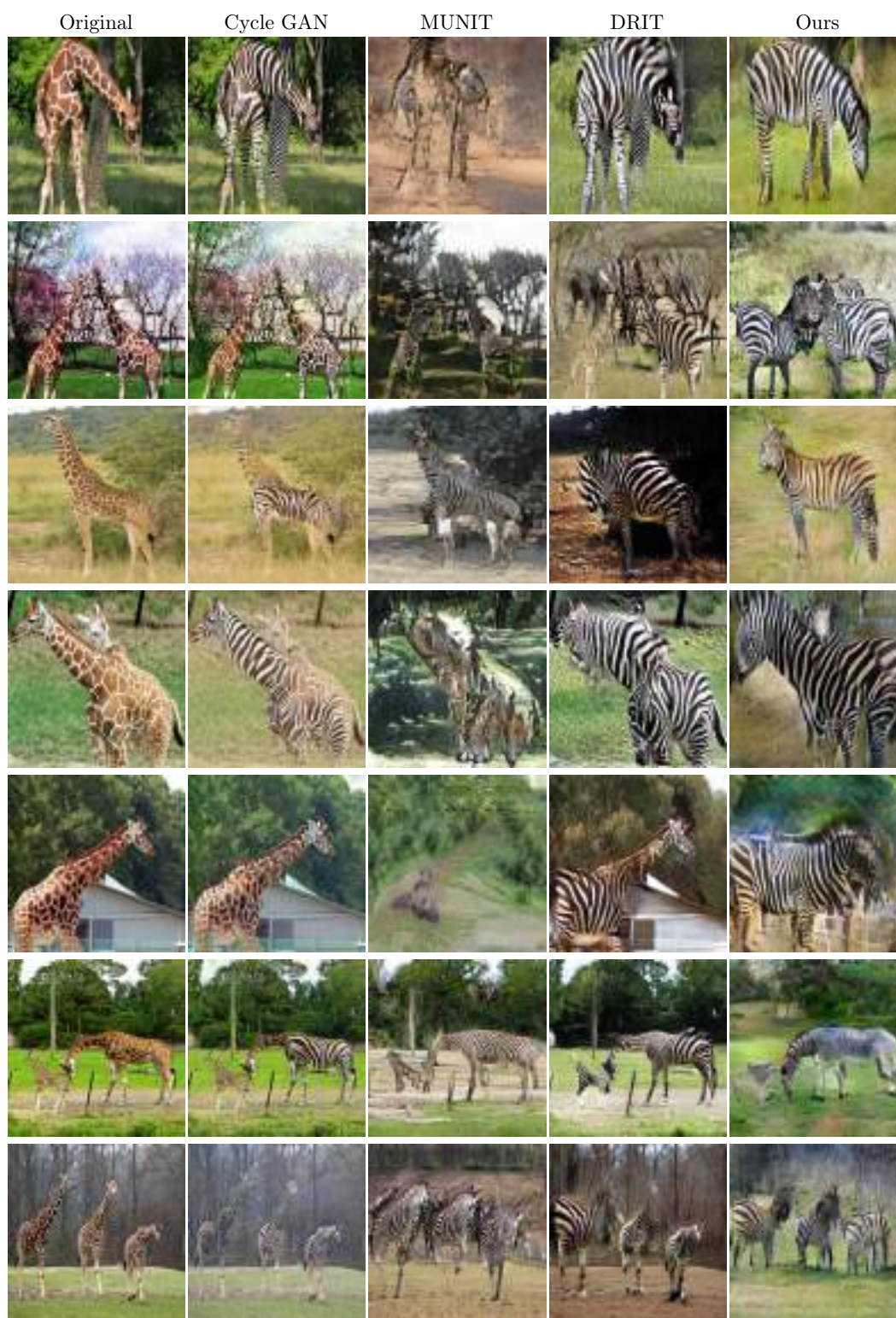
Figure S3: Qualitative comparisons. MSCOCO giraffe to zebra.

Original	Cycle GAN	MUNIT	DRIT	Ours

Figure S4: Qualitative comparisons. MSCOCO giraffe to zebra.

Original	Cycle GAN	MUNIT	DRIT	Ours
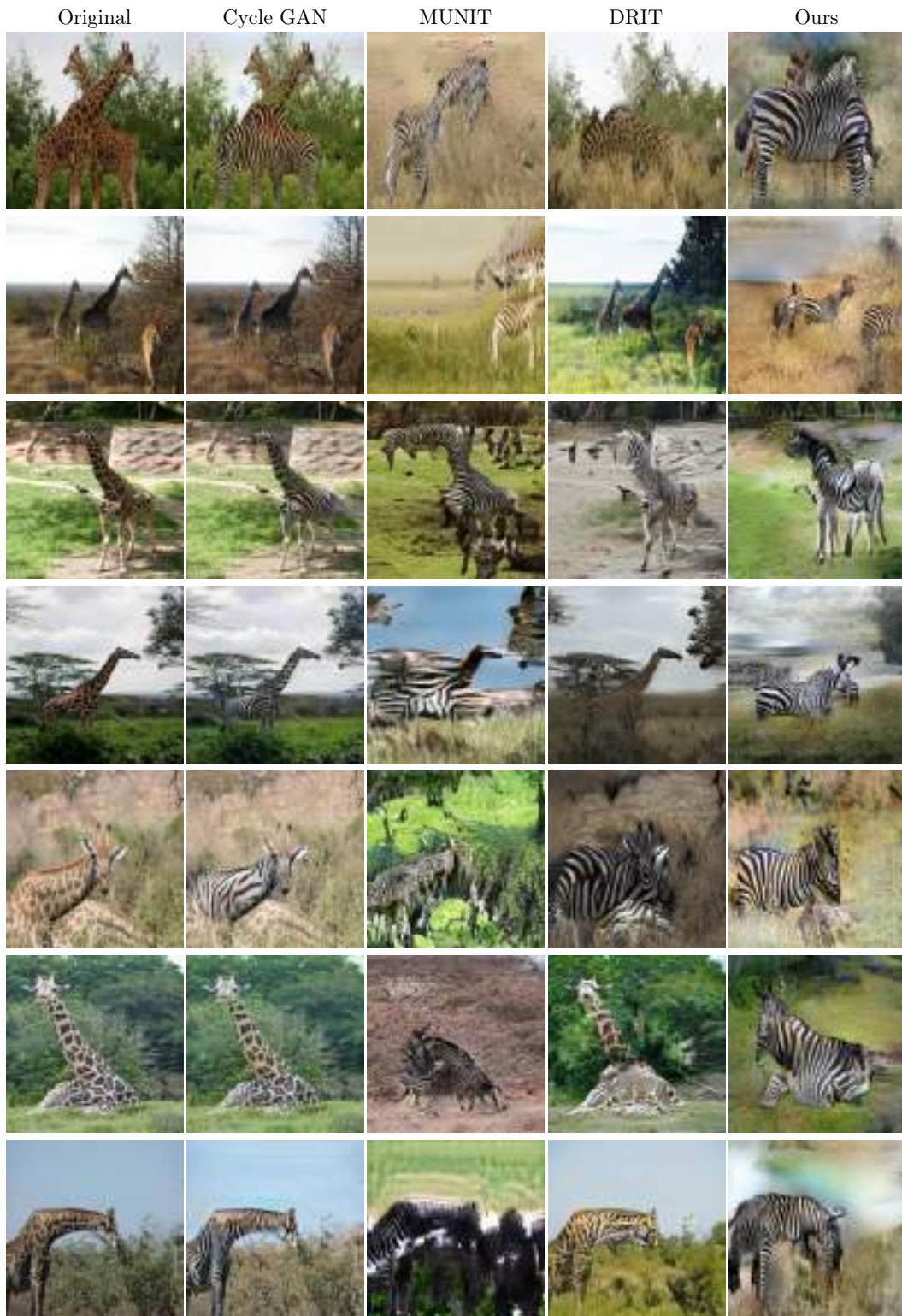
Figure S5: Qualitative comparisons. zebra to elephant.

Original　　　Cycle GAN　　　MUNIT　　　DRIT　　　Ours

Figure S6: Qualitative comparisons. zebra to elephant.

Original	Cycle GAN	MUNIT	DRIT	Ours

Figure S7: Qualitative comparisons. MSCOCO elephant to zebra.

Original	Cycle GAN	MUNIT	DRIT	Ours

Figure S8: Qualitative comparisons. MSCOCO elephant to zebra.

Original	Cycle GAN	MUNIT	DRIT	Ours

Figure S9: Qualitative comparisons. Kaggle cat to dog.

Original	Cycle GAN	MUNIT	DRIT	Ours
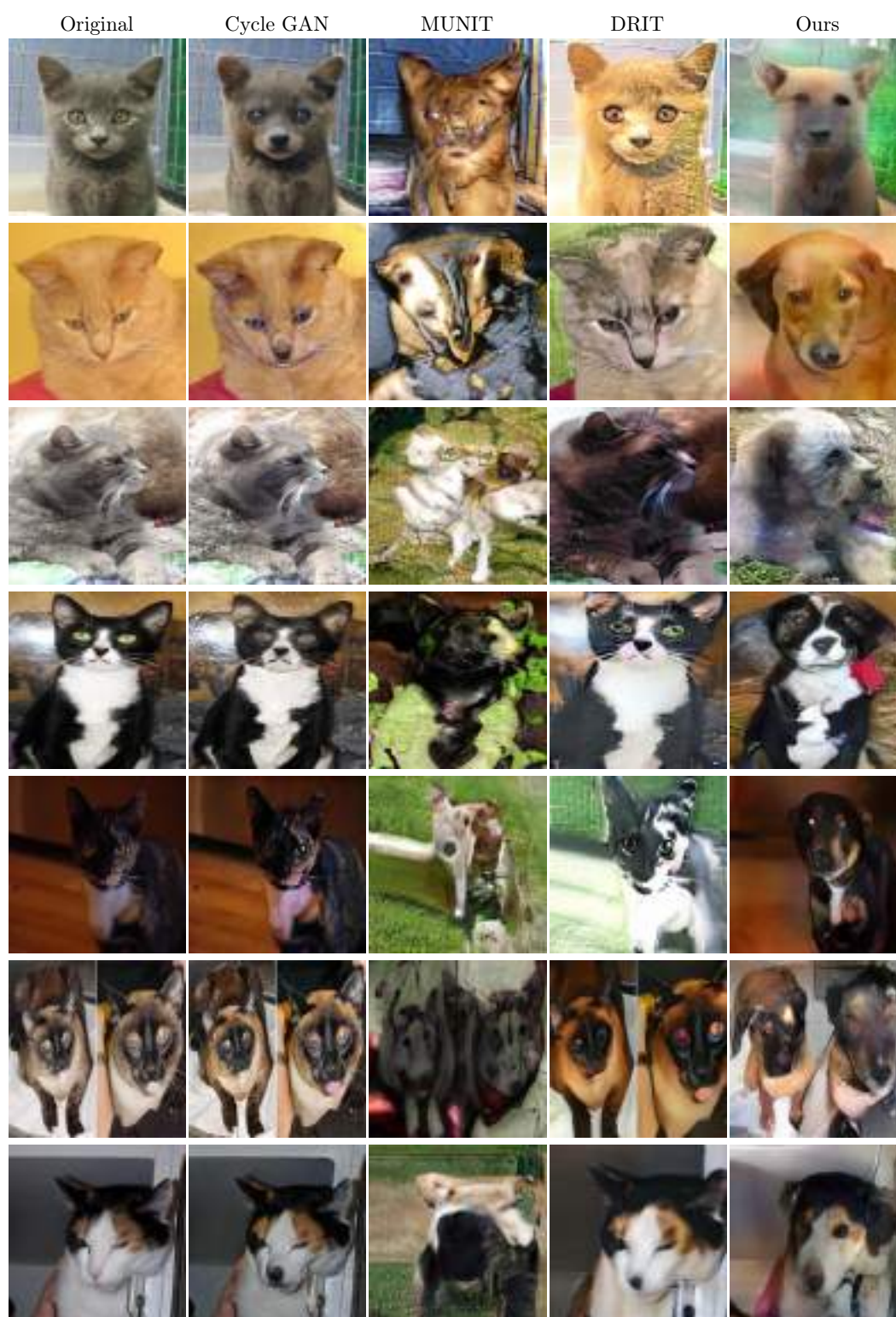
Figure S10: Qualitative comparisons. Kaggle cat to dog.

Original Cycle GAN MUNIT DRIT Ours
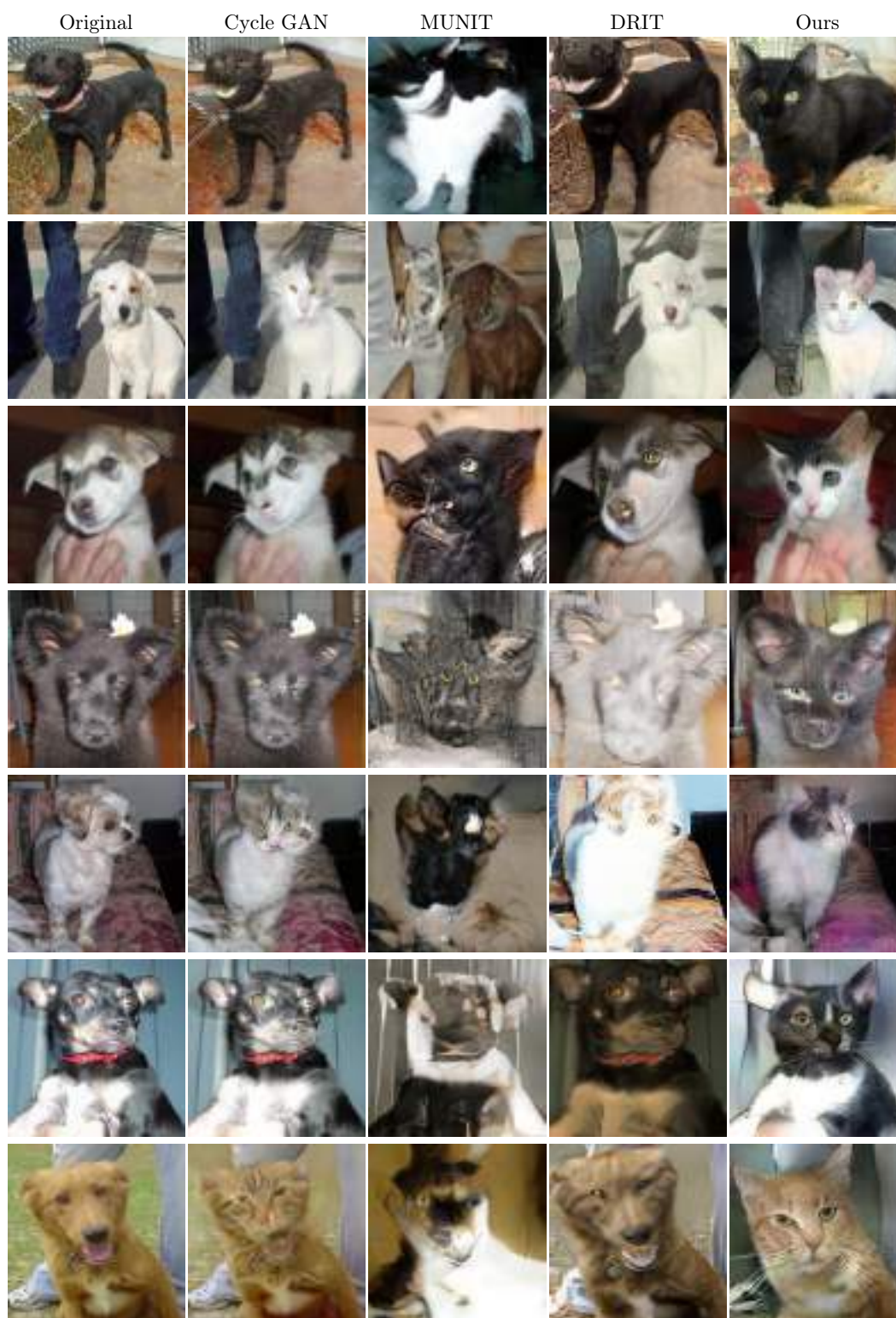
Figure S11: Qualitative comparisons. Kaggle dog to cat.

Original	Cycle GAN	MUNIT	DRIT	Ours

Figure S12: Qualitative comparisons. Kaggle dog to cat.

6.3 Non-shape deformation translation

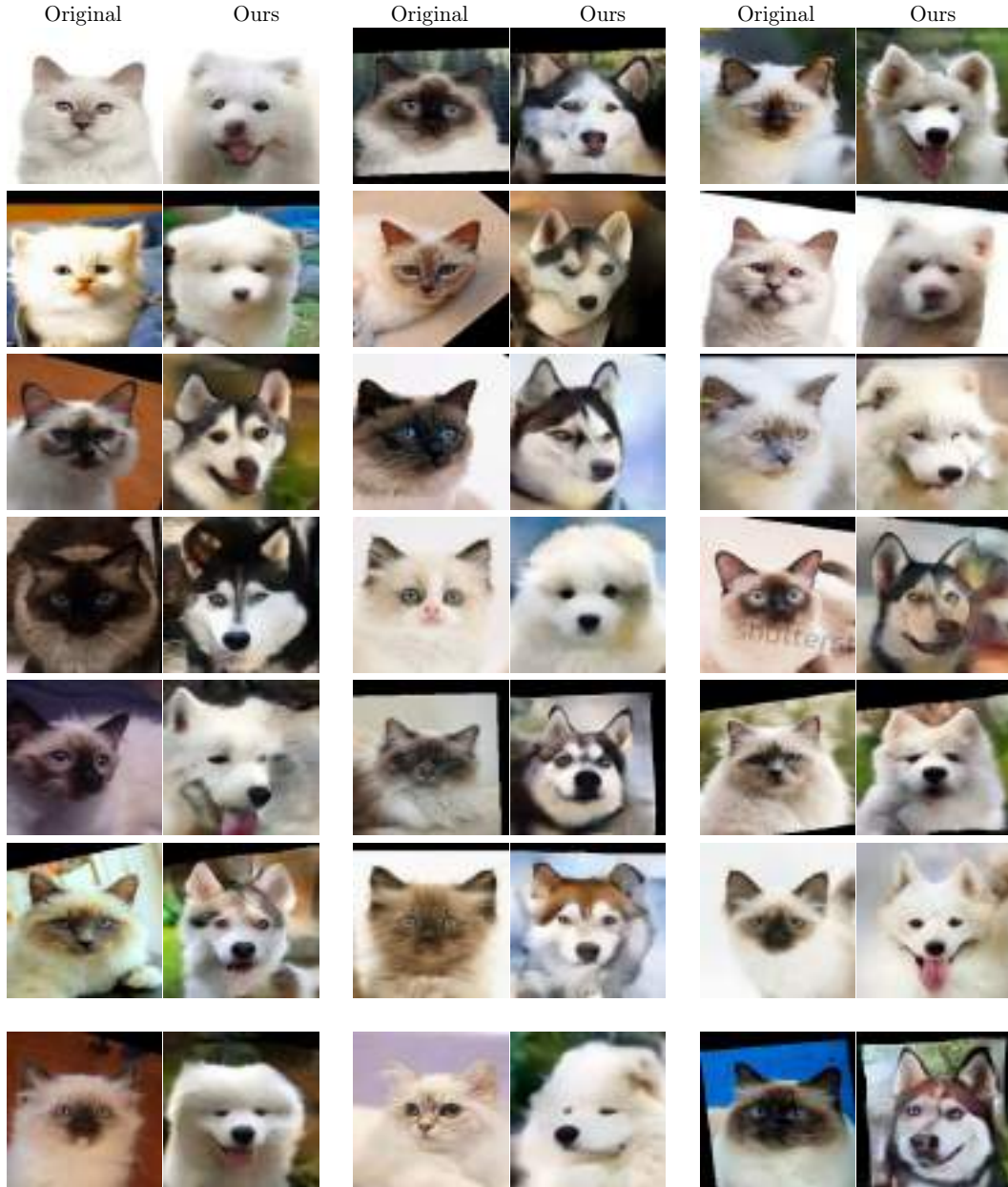Our method is also suited to none-shape deformation tasks, as in the case of dataset(1).

Original   Ours   Original   Ours   Original   Ours

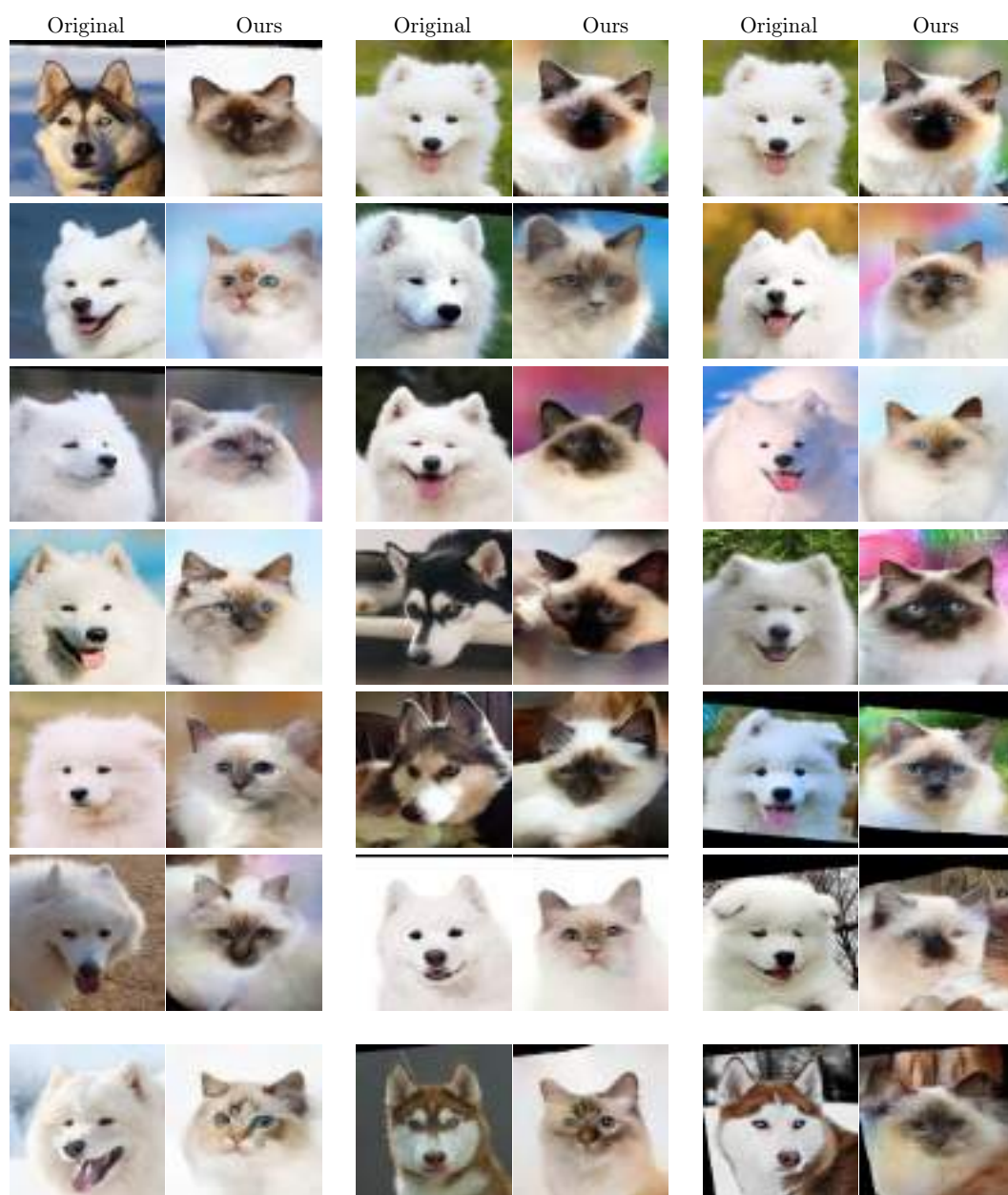Figure S13: Translation results from cats to dogs (faces).

Figure S14: Translation results from dogs to cats (faces).

6.4 Coarse to fine translation

We here present the translation of each layer. The translation of each shallower layer is conditioned on the translation result of the previous layer, and learns to add fine scale and appearance, such as texture. At every layer, in order to visualize the generated deep features, we use a network pre-trained for inverting the deep features of VGG-19, following the method of Dosovitskiy and Brox [5].
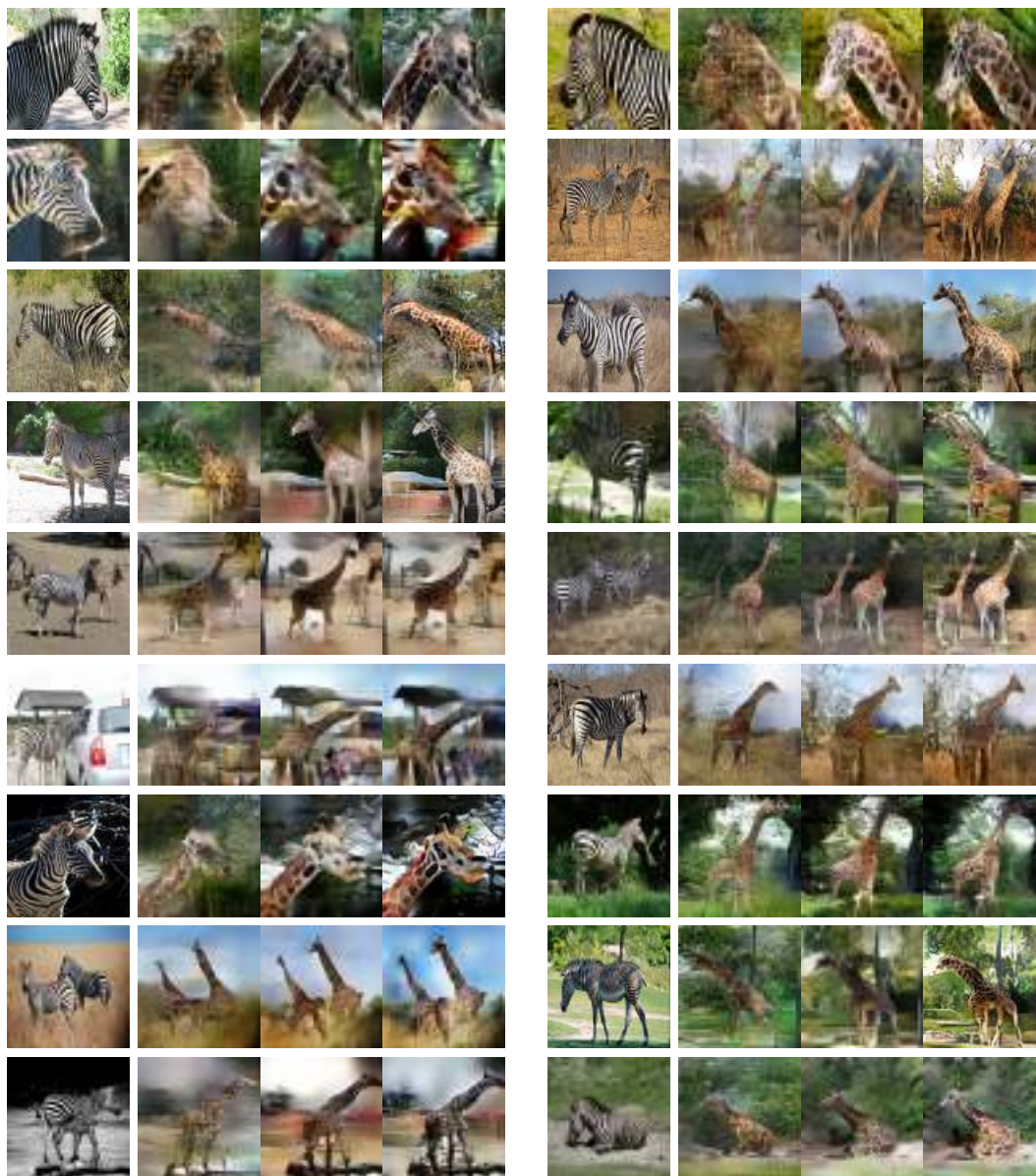

Figure S15: Coarse to fine translation of zebra to giraffe. Two different examples are shown in each row. The original image (left) is translated by the deepest translator (second left) and then in coarse to fine manner, shallower layers are translated (second right and most right).
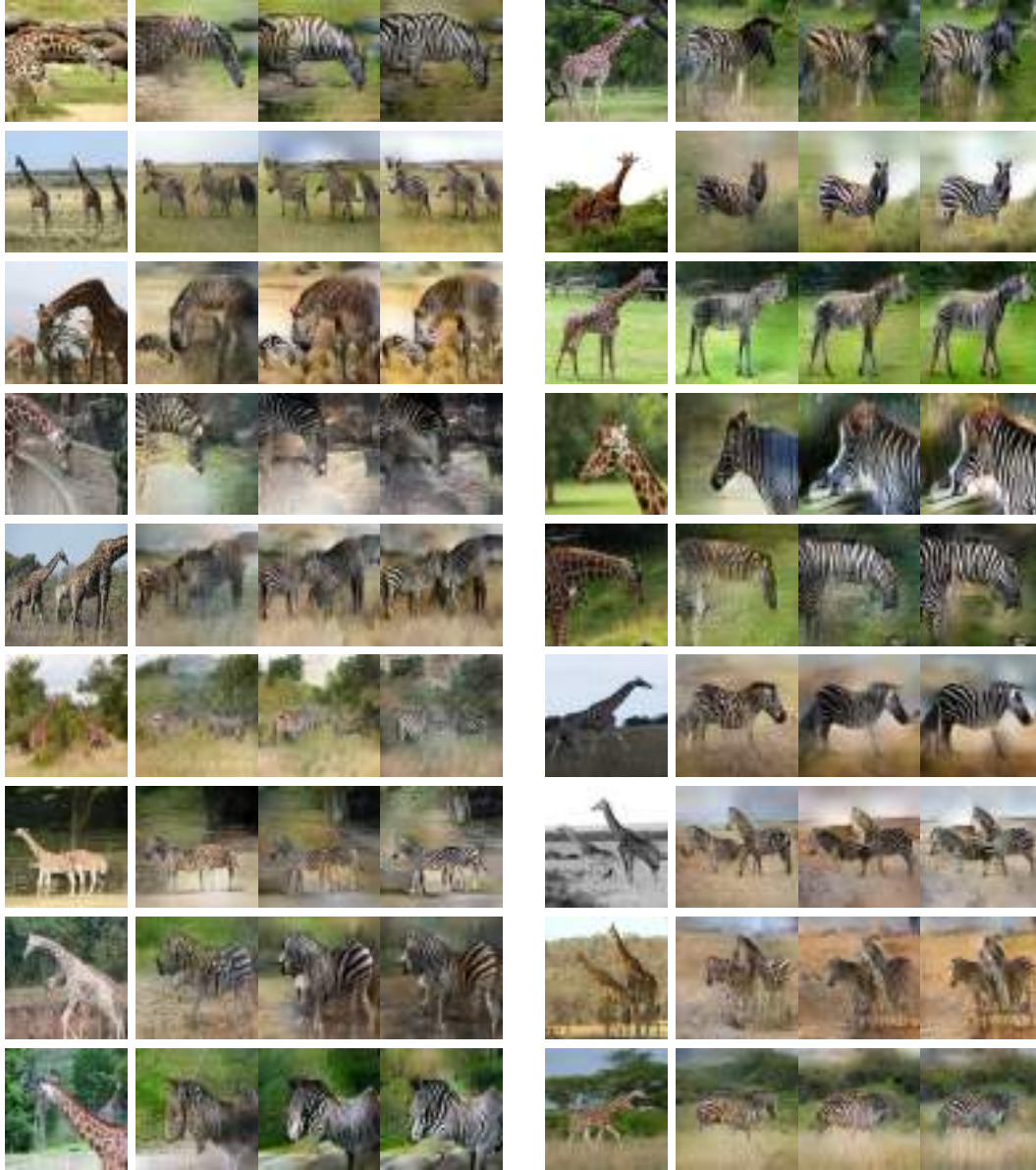
Figure S16: Coarse to fine translation of giraffe to zebra. Two different examples are shown in each row. The original image (left) is translated by the deepest translator (second left) and then in coarse to fine manner, shallower layers are translated (second right and most right).

6.5   Nearest neighbor comparison

In this section we show side by side, source images, our translation and the three nearest neighbors in the target domain. We use the LPIPS metric, presented in "The Unreasonable Effectiveness of Deep Features as a Perceptual Metric" by Zhang et al. This metric is based on L_2 distance of deep features extracted from pre-trained network. In our case we use the default settings proposed by Zhang et al. (i.e. alex net). As we show, the closest image in the target dataset vary in pose, scale and content (i.e. different parts of the objects).

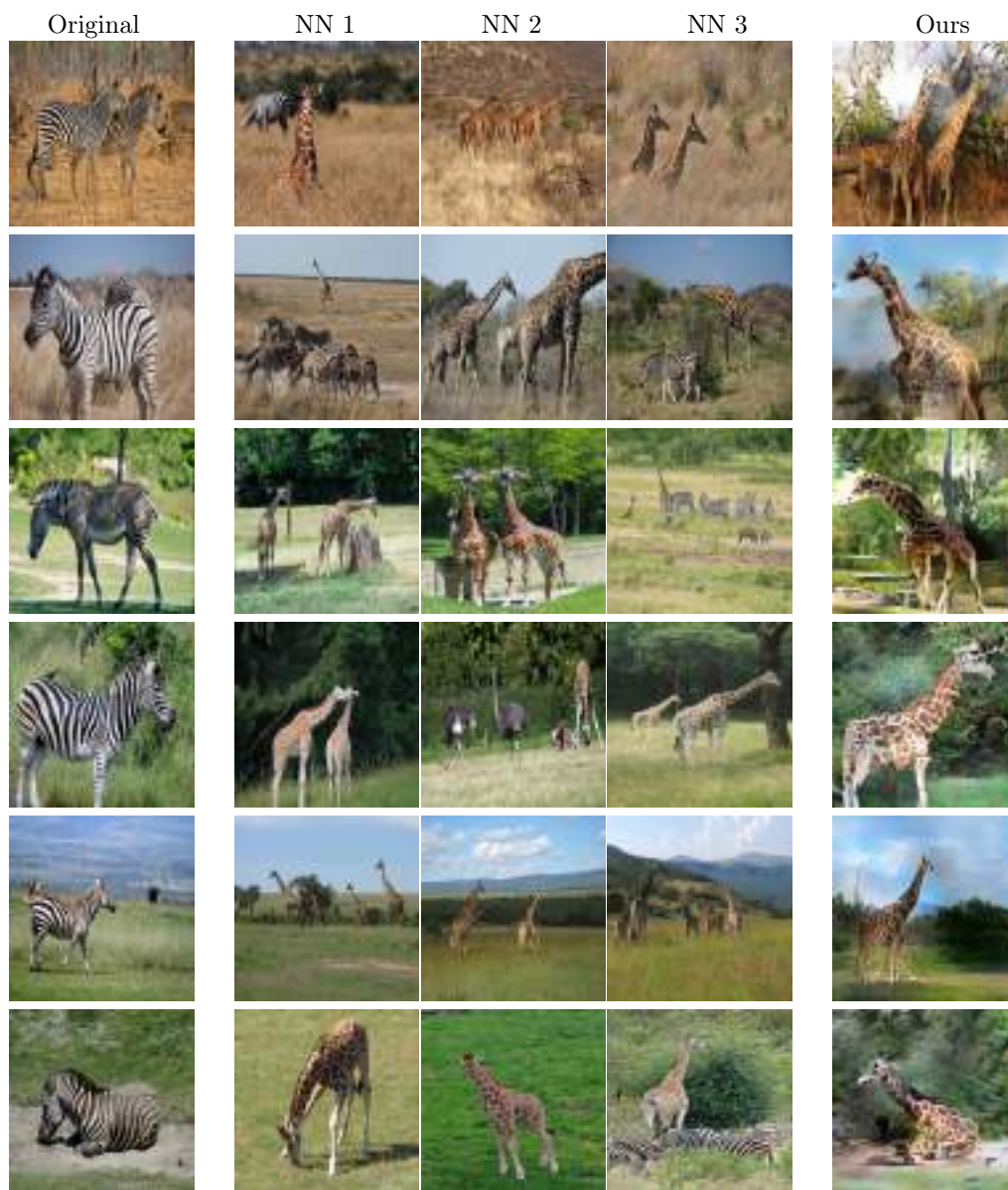| Original	NN 1	NN 2	NN 3	Ours

Figure S17: Nearest neighbor comparison to our result for zebra to giraffe translation. The NNs were found by exhaustive search on all the giraffe dataset using perceptual metric (LPIPS). The closest giraffe to the source zebra vary in scale, position and content

Figure S18: Nearest neighbor comparison to our result for giraffe to zebra translation. The NNs were found by exhaustive search on all the giraffe dataset using perceptual metric (LPIPS). The closest zebra to the source giraffe vary in scale, position and content.